Analytical solutions for gravity changes caused by triaxial volumetric sources

Mehdi Nikkhoo[1], Eleonora Rivalta[1,2]

[1]GFZ German Research Centre for Geosciences, Potsdam, Germany.
[2]Department of Physics and Astronomy, Alma Mater Studiorum University of Bologna, Italy.

Key Points:

- We develop analytical solutions for gravity changes due to the point Compound Dislocation Model (point CDM) simulating triaxial expansions
- Fully-coupled rapid inversions of deformation and gravity changes, accounting for deformation-induced gravity changes are now possible
- Gravity changes together with either horizontal or vertical displacements can constrain deformation source parameters and mass change

Corresponding author: Mehdi Nikkhoo, `mehdi.nikkhoo@gfz-potsdam.de`

Corresponding author: Eleonora Rivalta, `eleonora.rivalta@unibo.it`

Abstract

Volcanic crises are often associated with magmatic intrusions or pressurization of magma chambers of various shapes. These volumetric deformation sources dilate the country rocks changing their density, and cause uplift. Both the net mass of intruding magmatic fluids and these deformation effects contribute to surface gravity changes. Thus, to estimate the intrusion mass from gravity changes the deformation effects must be accounted for. We develop point-source analytical solutions and computer codes for the gravity changes caused by triaxial sources of expansion. This establishes fully coupled solutions for joint inversions of deformation and gravity changes. Such inversions can constrain both the intrusion mass and the deformation source parameters more accurately. In the absence of vertical displacement data, gravity changes together with horizontal displacements can be inverted to retrieve both the intrusion mass and the deformation source parameters.

Plain Language Summary

Volcanic crises are usually associated with magmatic fluids that intrude and deform the host rocks before potentially breaching the Earth's surface. It is important to estimate how much fluid (mass and volume) is on the move. Volume can be determined from the measured surface uplift. Mass can be determined from surface gravity changes. The fluid intrusion increases the mass below the volcano, thereby increasing the gravity, and pressurizes the rocks. This dilates parts of the host rock and compresses other parts, changing the rock density and redistributing the rock mass. This causes secondary gravity changes, called deformation-induced gravity changes. The measured gravity change is always the sum of the mass and deformation-induced contributions. Here we develop mathematical equations for rapid estimation of these deformation-induced gravity changes caused by arbitrary intrusion shapes. This way we can tell the mass contribution apart from the deformation contribution. We show that by using this solution not only the intrusion mass, but also other intrusion parameters including the volume, depth and shape can be calculated more accurately. This work extends the role of volcano gravimetry beyond its conventional role, allowing the gravimeters to play a role similar to that of the GPS.

1 Introduction

Intrusion of magma through the host rock or into an existing magma chamber deforms the Earth's crust and also changes the surface gravity field. The intrusion mass is a key information for characterizing the nature of the activity and its possible future evolution. Joint analyses of the measured surface displacements and gravity changes can constrain the intrusion mass, beside the other parameters of the deformation source, that is, its location, shape, spatial orientation, and some strength parameter (pressure or volume change; Okubo et al., 1991; Battaglia et al., 1999, 2003).

Both the mass transport and the ensuing country-rock deformations contribute to the gravity changes (Hagiwara, 1977; Walsh & Rice, 1979; Bonafede & Mazzanti, 1998; Lisowski, 2007). Such deformation-induced effects may be substantial for non-spherical sources, as shown through numerical models based on the finite element method (FEM; see Currenti et al., 2007, 2008; Trasatti & Bonafede, 2008; Currenti, 2014). The deformation effects caused by tabular sources such as dikes and sills can be estimated through the Okubo (1992) analytical solutions. There are no analytical solutions for other source geometries, such as ellipsoids, yet rigorous joint inversions of surface displacements and gravity changes demand fully-coupled models accounting for the source shape (Amoruso et al., 2008).

A source model composed of three orthogonal tensile dislocations can simulate the deformation field associated with triaxial sources (Lisowski et al., 2008; Bonafede & Fer-

rari, 2009; Amoruso & Crescentini, 2013). Based on this concept, Nikkhoo et al. (2017) developed the point Compound Dislocation Model (point CDM), which represents the far-field deformation of generic triaxial sources. This source model spans a wider parameter space than ellipsoids (Ferrari et al., 2015) while retaining the simplicity of the Mogi (1958) model.

In this study we use the Okubo (1991) expressions to derive analytical solutions for the gravity changes associated with the point CDM. We show how gravity changes due to point and finite ellipsoidal sources can be calculated by using the point CDM. We compare the point CDM gravity changes with the Hagiwara (1977) and Trasatti and Bonafede (2008) solutions. Finally, we elaborate on the potential of the model for coupled inversions of surface displacements and gravity changes.

2 Methods

In the following we assume a homogeneous, isotropic elastic half-space as a model for the Earth's crust. We denote the Poisson's ratio, shear modulus and bulk modulus in the medium by ν, μ and K, respectively. We adopt a right-handed xyz Cartesian coordinate system with the origin at the free surface and the z axis pointing upward. By "gravity change" we refer to the change in the absolute value of the gravity vector's z component. Thus, a positive mass change (mass increase) below a gravimeter leads to a positive gravity change (gravity increase).

2.1 Gravity changes caused by magma chamber pressurization

Suppose that magma degassing pressurizes a magma chamber (Figure 1). We assume that the exsolved gases all gather at the interface between the chamber walls and the degassed magma, forming a shell-shaped cavity. The formation of this interface cavity is accompanied by outward expansion of the chamber walls and inward compression of the magma, leading to the oppositely signed chamber volume change, δV_c, and magma volume change, δV_m, respectively. The total volume created by the expansion-compression process—namely, the interface volume change, ΔV_int—is given by

$$\Delta V_\mathrm{int} = \delta V_\mathrm{c} - \delta V_\mathrm{m}, \tag{1}$$

or equivalently by

$$\Delta V_\mathrm{int} = V_\mathrm{c} - V_\mathrm{m}, \tag{2}$$

where $V_\mathrm{c} = V + \delta V_\mathrm{c}$ and $V_\mathrm{m} = V + \delta V_\mathrm{m}$ are the chamber volume and magma volume in the deformed state, respectively, and V represents both the chamber volume and magma volume in the undeformed state. The chamber expansion also uplifts the surface by δh and generates a strain field, ϵ_{ij}, in the surrounding rocks. This changes the density of the rocks by $\delta\rho_\mathrm{r} = -\rho_\mathrm{r}\epsilon_{kk}$, where ρ_r is the rock density in the undeformed state and $\epsilon_{kk} = \epsilon_{11} + \epsilon_{22} + \epsilon_{33}$ is the volumetric strain or dilatation—a positive dilatation reduces the density (see Figure 1). Similarly, the magma density change, $\delta\rho_\mathrm{m}$, due to the compression is related to the magma compressibility, β_m, through $\delta\rho_\mathrm{m} = \rho_\mathrm{m}\beta_\mathrm{m}\delta p$, where ρ_m is the magma density in the undeformed state and δp is the pressure change in the chamber (Rivalta & Segall, 2008). Provided that β_m and δp are known, we have

$$\delta V_\mathrm{m} = V\beta_\mathrm{m}\delta p. \tag{3}$$

The density change in the δV_c portion is $-\rho_\mathrm{r}$ and the density change in the δV_m portion is $-\rho_\mathrm{m}$. The other zone of substantial density change is the Earth's surface, where areas of uplift and subsidence are subjected to density changes $+\rho_\mathrm{r}$ and $-\rho_\mathrm{r}$, respectively.

The same deformation-induced density changes exist if instead of exsolved gases, the interface cavity is formed by, and filled with, the intrusion of some external fluids.
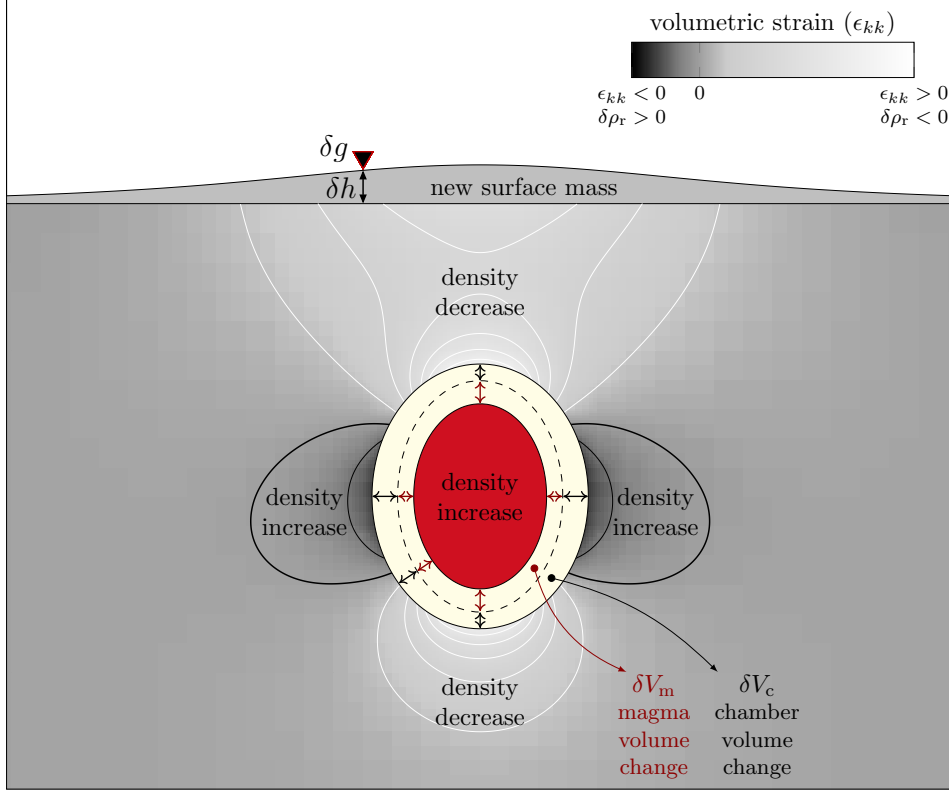
Figure 1. Schematic mass redistribution and surface uplift caused by chamber pressurization. Compressed magma (red) is surrounded by the interface cavity. The dashed ellipse depicts chamber walls prior to pressurization and separates the δV_{m} and δV_{c} portions of the interface cavity (see equation 1). The country rocks are subjected to positive dilatation/density decrease (light gray and white contours) and negative dilatation/density increase (dark gray and black contours). Thick black contour marks zero dilatation. Due to the uplift a mass layer is added to the surface and a gravity station (black triangle) has moved upward by δh.

In such case, the interface cavity is filled with a net mass

$$\Delta M = \rho_{\mathrm{int}} \Delta V_{\mathrm{int}}, \tag{4}$$

where ρ_{int} is the intrusion density.

In general, magma chamber expansions involve the following surface gravity change contributions:

1. Δg_{β}, due to density change $\delta \rho_{\mathrm{m}}$ in the magma volume in the deformed state, V_{m},
2. $\Delta g_{\delta V_{\mathrm{m}}}$, due to density change $-\rho_{\mathrm{m}}$ within the δV_{m} volume,
3. $\Delta g_{\delta V_{\mathrm{c}}}$, due to density change $-\rho_{\mathrm{r}}$ within the δV_{c} volume,
4. $\Delta g_{\epsilon_{kk}}$, due to density changes $\delta \rho_{\mathrm{r}}$ throughout the country rocks,
5. Δg_{SM}, due to addition of a surface mass layer with density $+\rho_{\mathrm{r}}$ and thickness δh during the uplift,
6. Δg_{FA}, due to the free air change in gravity associated with δh,
7. $\Delta g_{\Delta M}$, due to the added intrusion mass ΔM that leads to density change ρ_{int} within the interface cavity,

for a total surface gravity change of

$$\delta g = \Delta g_\beta + \Delta g_{\delta V_{\mathrm{m}}} + \Delta g_{\delta V_{\mathrm{c}}} + \Delta g_{\epsilon_{kk}} + \Delta g_{\mathrm{SM}} + \Delta g_{\mathrm{FA}} + \Delta g_{\Delta M}. \tag{5}$$

We can estimate the intrusion mass from $\Delta g_{\Delta M}$ in equation (5); however, this requires all the other terms in equation (5) to be quantified first. δg can be determined through repeated gravity measurements. Also, from repeated geodetic measurements δh can be determined, from which Δg_{FA} can be estimated as

$$\Delta g_{\mathrm{FA}} = \gamma \delta h, \tag{6}$$

where $\gamma \simeq -0.3086 \times 10^{-5}\,\mathrm{s}^{-2}$ is the free air gradient; and also, for flat topographies Δg_{SM} can be estimated from

$$\Delta g_{\mathrm{SM}} = 2\pi G \rho_{\mathrm{r}} \delta h, \tag{7}$$

where G is the gravitational constant. The other terms in equation (5) can be estimated only by using a deformation model for the chamber pressurization. It is useful to regroup these subsurface contributions as

$$\Delta g_{\Delta V_{\mathrm{int}}} = \Delta g_{\delta V_{\mathrm{c}}} + \Delta g_{\delta V_{\mathrm{m}}}, \tag{8}$$

where $\Delta g_{\Delta V_{\mathrm{int}}}$ is the contribution of the interface cavity (see equation 1), and as

$$\Delta g_{\mathrm{MD}} = \Delta g_\beta + \Delta g_{\epsilon_{kk}}, \tag{9}$$

where Δg_{MD} is the contribution of the medium dilatation in both the country rocks and magma chamber.

2.1.1 The far field approximations

The far field gravity changes caused by the intruded fluid mass can be calculated through a point-mass approximation as

$$\Delta g_{\Delta M} = G \Delta M \frac{d}{r^3}, \tag{10}$$

where d is the depth to the center of the chamber and r is the distance between the canter of the chamber and the surface observation point. This approximation can be applied also to the far field gravity changes caused by the other density changes in the chamber, as

$$
\begin{aligned}
\Delta g_\beta &= G \delta\rho_{\mathrm{m}} V_{\mathrm{m}} \frac{d}{r^3}, \\
\Delta g_{\delta V_{\mathrm{m}}} &= G \rho_{\mathrm{m}} \delta V_{\mathrm{m}} \frac{d}{r^3}, \\
\Delta g_{\delta V_{\mathrm{c}}} &= -G \rho_{\mathrm{r}} \delta V_{\mathrm{c}} \frac{d}{r^3}, \\
\Delta g_{\Delta V_{\mathrm{int}}} &= -G \rho_{\mathrm{r}} \Delta V_{\mathrm{int}} \frac{d}{r^3}.
\end{aligned}
\tag{11}
$$

The conservation of the initial magma mass in the chamber implies $\delta\rho_{\mathrm{m}} V_{\mathrm{m}} = -\rho_{\mathrm{m}} \delta V_{\mathrm{m}}$, which together with equation (11) yields

$$\Delta g_\beta + \Delta g_{\delta V_{\mathrm{m}}} = 0. \tag{12}$$

This leads to the simplified, far-field form of equation (5)

$$\delta g = \Delta g_{\delta V_{\mathrm{c}}} + \Delta g_{\epsilon_{kk}} + \Delta g_{\mathrm{SM}} + \Delta g_{\mathrm{FA}} + \Delta g_{\Delta M}, \tag{13}$$

which states that the far field gravity changes caused by the pressurization of the chamber (the deformation effects) are not sensitive to the density and compressibility of the
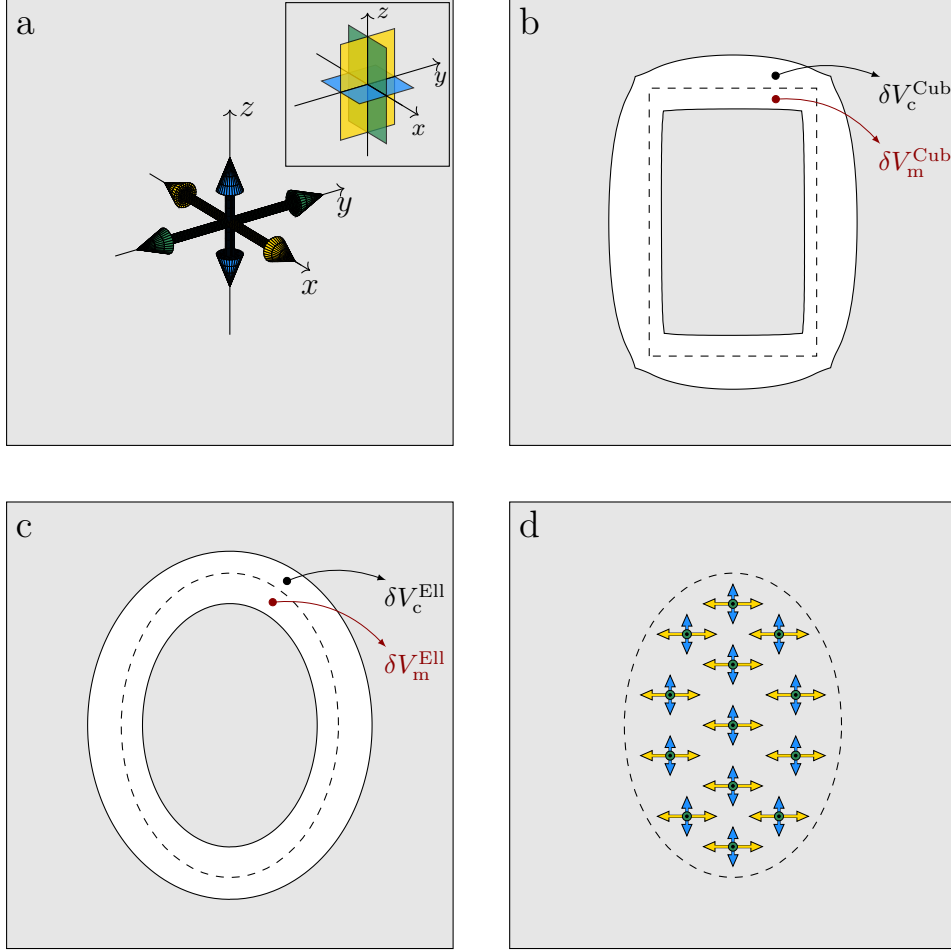
Figure 2. Triaxial volumetric sources. a) A point CDM with potencies ΔV_x (yellow), ΔV_y (green) and ΔV_z (blue), where $\Delta V_x = \Delta V_y > \Delta V_z$. Inlet shows the equivalent CDM (see Nikkhoo et al., 2017). b) A uniformly pressurized cuboidal source with $K_{\mathrm{m}} = K$. The two interface cavity portions $\delta V_{\mathrm{c}}^{\mathrm{Cub}}$ and $\delta V_{\mathrm{m}}^{\mathrm{Cub}}$ are indicated, where $\Delta V^{\mathrm{Cub}} = \delta V_{\mathrm{c}}^{\mathrm{Cub}} + \delta V_{\mathrm{m}}^{\mathrm{Cub}}$. c) Same as (b), but for a uniformly pressurized ellipsoidal source. The interface cavity portions are $\delta V_{\mathrm{c}}^{\mathrm{Ell}}$ and $\delta V_{\mathrm{m}}^{\mathrm{Ell}}$, with $\Delta V^{\mathrm{Ell}} = \delta V_{\mathrm{c}}^{\mathrm{Ell}} + \delta V_{\mathrm{m}}^{\mathrm{Ell}}$. Note that $\delta V_{\mathrm{c}}^{\mathrm{Cub}} \neq \delta V_{\mathrm{c}}^{\mathrm{Ell}}$ and $\delta V_{\mathrm{m}}^{\mathrm{Cub}} \neq \delta V_{\mathrm{m}}^{\mathrm{Ell}}$ but $\Delta V^{\mathrm{Cub}} = \Delta V^{\mathrm{Ell}}$. d) A set of N point CDMs uniformly distributed within the ellipsoidal cavity in c. The point CDM in (a) represents the far field of all the finite sources in (b), (c) and (d). Provided $N \to \infty$, the near fields of (c) and (d) are equivalent.

chamber contents. Thus, simulating the magma chamber as a pressurized cavity or as a pressurized chamber filled with some arbitrary material, both yield the same results for $\Delta g_{\delta V_c} + \Delta g_{\epsilon_{kk}}$.

In the derivation of equations (1–13) no assumptions on the magma chamber shape are necessary; thus, these equations are valid for any magma chamber shape.

2.2 Gravity changes caused by the point CDM

The Nikkhoo et al. (2017) point CDM represents the far field of triaxial sources of expansion with arbitrary spatial orientations. The point CDM is composed of three mutually orthogonal point tensile dislocations (see Figure 2a) constrained to either expand or contract together. The strength of each point tensile dislocation is determined by its potency, defined as the product of dislocation surface and opening (Aki & Richards, 2002; Nikkhoo et al., 2017, see also Appendix A). The point CDM has 10 parameters: 3 location coordinates, 3 rotation angles, 3 potencies specifying the expansion intensity along the three principal axes of the source, and ν. The total potency of the point CDM, denoted by ΔV, is the sum of the three potencies. ΔV has the units of volume but it is only a measure of the source strength and it represents the volume of the interface cavity, that is, $\Delta V = \Delta V_{\text{int}}$, provided that $K_{\text{m}} = K$, where $K_{\text{m}} = 1/\beta_{\text{m}}$ is the bulk modulus of magma.

Triaxial sources of differing shapes, but identical far field deformation, have the same point CDM representation. However, in order to have the same δV_{c} these sources must have also identical shapes. For example, the uniformly-pressurized cuboidal and ellipsoidal chambers in Figure 2 have the same potencies but their volume changes are different.

Gravity changes caused by arbitrary point tensile dislocations can be calculated through the Okubo (1991) analytical expressions (Appendix A). By superimposing the gravity changes associated with three mutually orthogonal point dislocations (equations A1–A2) we derive the analytical gravity changes associated with the point CDM as

$$\delta g = \Delta g_{\Delta V} + \Delta g_{\text{MD}} + \Delta g_{\text{SM}} + \Delta g_{\text{FA}} + \Delta g_{\Delta M}. \tag{14}$$

Calculating $\Delta g_{\delta V_{\text{c}}}$ requires knowledge of the chamber shape. As the point CDM does not assume any specific shape for the triaxial sources, the individual contributions $\Delta g_{\delta V_{\text{c}}}$ and $\Delta g_{\epsilon_{kk}}$ cannot be determined through the Okubo (1991) solutions. However, equations (8), (9) and (12), written for the point CDM, yield

$$\Delta g_{\text{MD}} + \Delta g_{\Delta V} = \Delta g_{\delta V_{\text{c}}} + \Delta g_{\epsilon_{kk}}. \tag{15}$$

Knowing from section 2.1.1 that the far field gravity changes are not sensitive to the properties of the chamber contents, equation (15) leads to

$$\Delta g_{\text{MD}} + \Delta g_{\Delta V_{\text{int}}} = \Delta g_{\delta V_{\text{c}}} + \Delta g_{\epsilon_{kk}}. \tag{16}$$

Combined with equation (15) it can be concluded that the δg from equation (14) and the δg from equation (13) are equivalent and thus, the point CDM can be used to separate the deformation effects from the total gravity changes in order to uniquely constrain ΔM.

2.2.1 Gravity changes caused by point and finite pressurized ellipsoidal cavities

For any point ellipsoidal model after Davis (1986) there is an equivalent point CDM, related to the elastic parameters of the medium and the ellipsoid semi-axes and pressure change through the Eshelby (1957) tensor (see Nikkhoo et al., 2017). Thus, equation (14) also holds for point ellipsoidal sources. By calculating δV_{c} for ellipsoidal cavities, again through the Eshelby (1957) tensor, $\Delta g_{\delta V_{\text{c}}}$ (equation 11) and thus, $\Delta g_{\epsilon_{kk}}$ (equation 15) can be determined for ellipsoidal sources.

Assume a point CDM with potencies $(\Delta V_a, \Delta V_b, \Delta V_c)$ represents the far field of a pressurized ellipsoidal cavity with semi-axes (a, b, c). Then, a set of N point CDMs with potencies $(\Delta V_a/N, \Delta V_b/N, \Delta V_c/N)$, uniformly distributed within the ellipsoid (see Figure 2d), approximates the near field deformations of the pressurized cavity (Eshelby, 1957;

Davis, 1986; Yang et al., 1988; Amoruso et al., 2008; Segall, 2010; Amoruso & Crescentini, 2011). Provided that $N \to \infty$, this procedure leads to an accurate solution, unless the cavity is immediately below the free surface (Yang et al., 1988; Segall, 2010; Amoruso & Crescentini, 2011). In practice, a few dozens of point CDMs already converge to satisfactory accuracies for most applications. The same procedure can be used to calculate the gravity changes caused by a finite pressurized ellipsoidal cavity.

3 Results

3.1 Comparisons with other gravity change solutions

Hagiwara (1977) derived closed-form expressions for the gravity change contributions caused by the Mogi (1958) source, later used to validate analytical (Okubo, 1991) and numerical solutions (Currenti et al., 2007, 2008; Trasatti & Bonafede, 2008).

An isotropic point CDM is equivalent to the Mogi (1958) model (Bonafede & Ferrari, 2009). Assuming potency $\Delta V^{(\mathrm{Mogi})}$ and depth d for such a point CDM, eq. A1 yields:

$$
\begin{aligned}
\Delta g_{\mathrm{MD}}^{(\mathrm{Mogi})} &= \frac{1}{3} G \rho_{\mathrm{r}} \left(1 - 2\nu\right) \Delta V^{(\mathrm{Mogi})} \frac{d}{r^3}, \\
\Delta g_{\mathrm{SM}}^{(\mathrm{Mogi})} &= \frac{2}{3} G \rho_{\mathrm{r}} \left(1 + \nu\right) \Delta V^{(\mathrm{Mogi})} \frac{d}{r^3}, \\
\Delta g_{\Delta V}^{(\mathrm{Mogi})} &= -G \rho_{\mathrm{r}} \Delta V^{(\mathrm{Mogi})} \frac{d}{r^3}.
\end{aligned}
\tag{17}
$$

Also, by using equations (11) and (15) and noting that $\Delta V^{(\mathrm{Mogi})} = \frac{3(1-\nu)}{(1+\nu)} \delta V_{\mathrm{c}}^{(\mathrm{Mogi})}$ (see Aki & Richards, 2002; Bonafede & Ferrari, 2009; Ichihara et al., 2016), we rewrite equations (17) in terms of $\delta V_{\mathrm{c}}^{(\mathrm{Mogi})}$:

$$
\begin{aligned}
\Delta g_{\epsilon_{kk}}^{(\mathrm{Mogi})} &= -G \rho_{\mathrm{r}} \left(1 - 2\nu\right) \delta V_{\mathrm{c}}^{(\mathrm{Mogi})} \frac{d}{r^3}, \\
\Delta g_{\mathrm{SM}}^{(\mathrm{Mogi})} &= 2 G \rho_{\mathrm{r}} \left(1 - \nu\right) \delta V_{\mathrm{c}}^{(\mathrm{Mogi})} \frac{d}{r^3}, \\
\Delta g_{\delta V_{\mathrm{c}}}^{(\mathrm{Mogi})} &= -G \rho_{\mathrm{r}} \delta V_{\mathrm{c}}^{(\mathrm{Mogi})} \frac{d}{r^3},
\end{aligned}
\tag{18}
$$

which are equivalent to the Hagiwara (1977) expressions, (see also Hagiwara, 1977; Rundle, 1978; Walsh & Rice, 1979; Savage, 1984; Okubo, 1991). This validates the gravity change solution for the point CDM in the case of point spherical cavities.

We now show that the gravity change solutions for the point CDM also provide a basis for rigorous benchmarking of numerical solutions. We use the point CDM and the N-point CDM to calculate the surface displacements (Figure 3a) and gravity changes (Figure 3b) associated with the Trasatti and Bonafede (2008) FEM solution for a pressurized vertical prolate spheroidal cavity.

In the far field, the point CDM and the N-point CDM displacements are undistinguishable. The FEM solution shows a small deviation which can be attributed to the finite domain of the model. In the near field, the N-point CDM and the FEM displacements show a very good agreement. The $\sim 8\%$ difference between the N-point CDM and the point CDM reflects the difference between a point-source and a finite-source solution.

There is also a good agreement between the gravity changes from all approaches (Figure 3b). The subtle differences between the N-point CDM and the FEM gravity change contributions reflect the errors in the FEM vertical displacements and cavity volume change, due to the FEM finite model size, discretized chamber walls, meshing of the domain. The largest difference between the Trasatti and Bonafede (2008) and the other solutions is slightly above 1 μGal, which is more than double the error that Trasatti and Bonafede

(2008) estimated by comparison with Hagiwara (1977). This suggests that comparing numerical models with the solution for spherical cavities only may underestimate the numerical computation errors.

3.2 The contribution of gravity changes for the retrieval of deformation source parameters

Dieterich and Decker (1975) showed that different source shapes produce almost undistinguishable uplift patterns if the source depth is appropriately adjusted. However, the associated horizontal displacements will be completely different. The implication is that in order to constrain all source parameters reliably, horizontal and vertical displacement data must be inverted together. Similar to horizontal and vertical surface displacements, the deformation-induced gravity changes depend on the deformation source parameters. Thus, gravity changes can potentially help better constrain them (Trasatti & Bonafede, 2008). We use the point CDM to simulate the radial and vertical displacements and the gravity changes associated with three different radially-symmetrical deformation sources: a horizontal sill, an isotropic source and a prolate source (see Figure 4).

The source depths in Figure 4a lead to similar vertical displacements (Figure 4c), but distinct horizontal displacements (Figure 4d). Note that the gravity changes (free air contribution removed) are also completely distinct (Figure 4b), and thus, together with the vertical displacements alone, can constrain the source shape and depth. Adjusting the source depths differently (Figure 4e) such that the horizontal displacements match (Figure 4h), leads to distinct vertical displacements (Figure 4f) and distinct gravity changes (Figure 4g). Thus, gravity changes together with horizontal displacements alone can also constrain the source parameters.

4 Discussion

Volcano gravity changes caused by the net mass of intruding magmatic fluids and the induced host rock deformations may have comparable magnitudes to those of hydrological origin, such as changes in the water table. Such hydrogravimetric disturbances can be corrected for by employing hydrological monitoring and modeling techniques (Battaglia et al., 2003, 2006; Creutzfeldt et al., 2010; Van Camp et al., 2010; Lien et al., 2014; Kazama et al., 2015) or by analyzing time-lapse gravity data (Güntner et al., 2017). Thus, the mass of intruding fluids at volcanoes can be inferred reliably once such effects are corrected for.

Low-cost and accurate gravimeters are providing gravity time series at volcanoes at an unprecedented spatio-temporal resolution (Carbone et al., 2017, 2020). Permanent networks provide opportunities for new insight on magmatic plumbing systems (Battaglia et al., 2008; Carbone et al., 2019). One main challenge associated with these developments is to perform both detailed Bayesian inferences for in-depth understanding of the volcano and rapid inversions for hazard assessment and early warning.

The available FEM gravity change models can incorporate various chamber shapes (Currenti et al., 2007, 2008; Trasatti & Bonafede, 2008; Currenti, 2014), the Earth's surface topography (Currenti et al., 2007; Charco et al., 2009), crustal density and material heterogeneities (Wang et al., 2006; Currenti et al., 2007, 2008; Trasatti & Bonafede, 2008), viscoelasticity of the Earth's crust (Currenti, 2018), self-gravitation effects (Fernández et al., 2001, 2005; Charco et al., 2005, 2006) and magma compressibility (Currenti, 2014). Besides difficulties in implementing the FEM such as meshing issues, this powerful method is computationally too demanding to be used for detailed inverse modelling. In contrast, the point CDM is a half-space model, but has already proven to be suitable for exploring the parameter space in both detailed Bayesian inferences (see Lundgren et al., 2017) and rapid and unsupervised inversions of deformation data (see Beauducel et al., 2020).
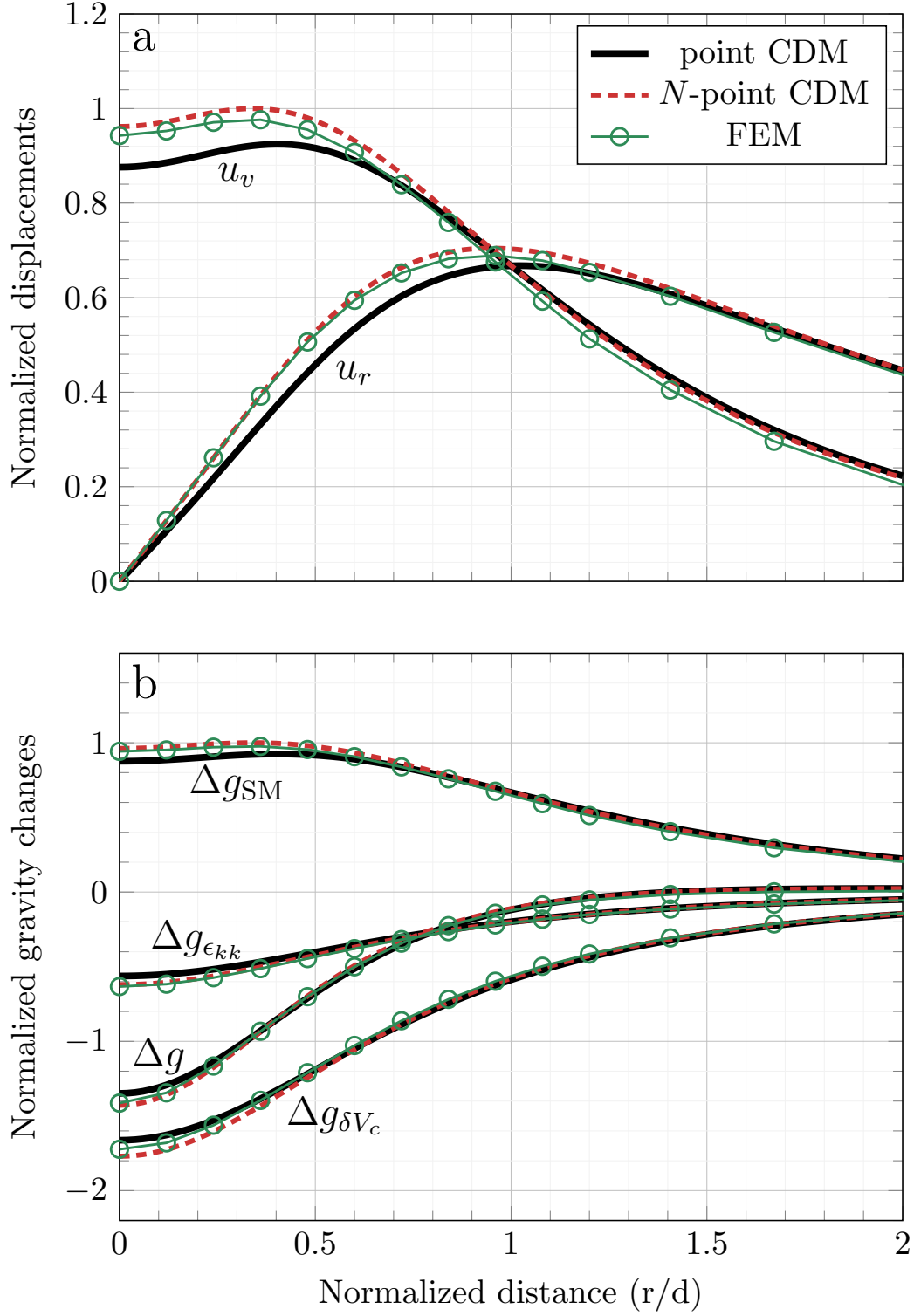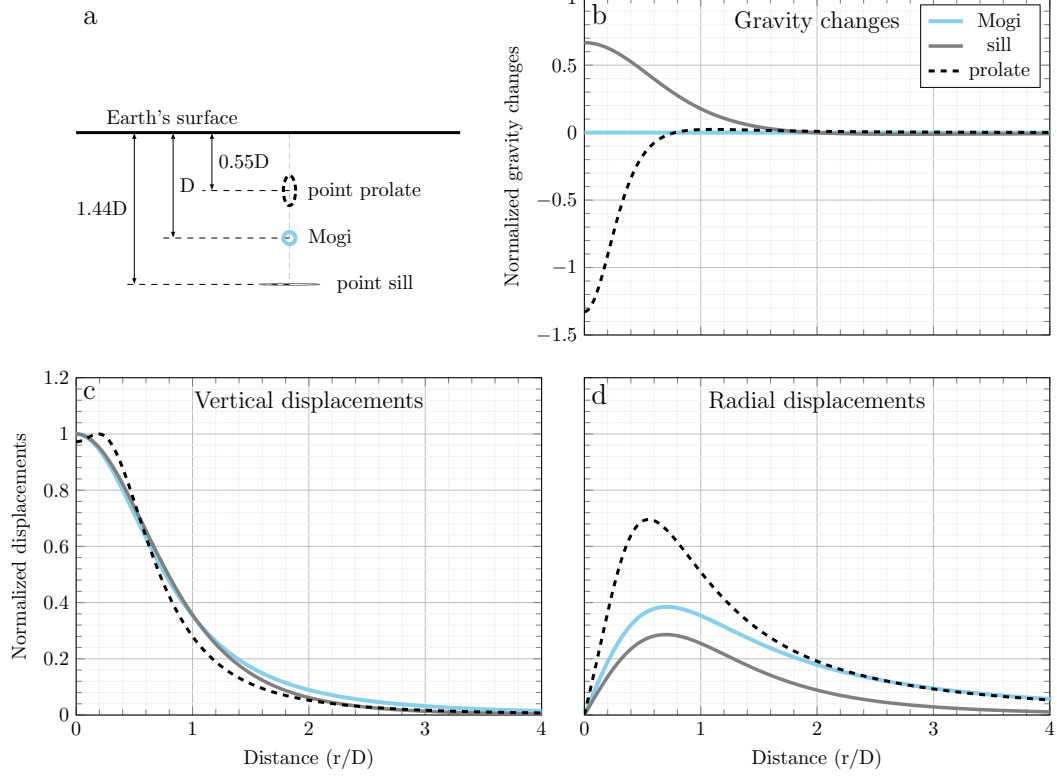
Figure 3. Comparing the point CDM and N-point CDM ($N \simeq 2 \times 10^5$) with the Trasatti and Bonafede (2008) FEM solution for a vertical prolate spheroidal cavity with semi-major axes 1.842 km, aspect ratio 0.4 and depth to the center 5 km. a) Radial (u_r) and vertical (u_v) displacements, normalized by the maximum vertical displacement of the N-point CDM solution. b) Gravity change contributions, normalized by the maximum Δg_{SM} of the N-point CDM solution.

Similar vertical displacements
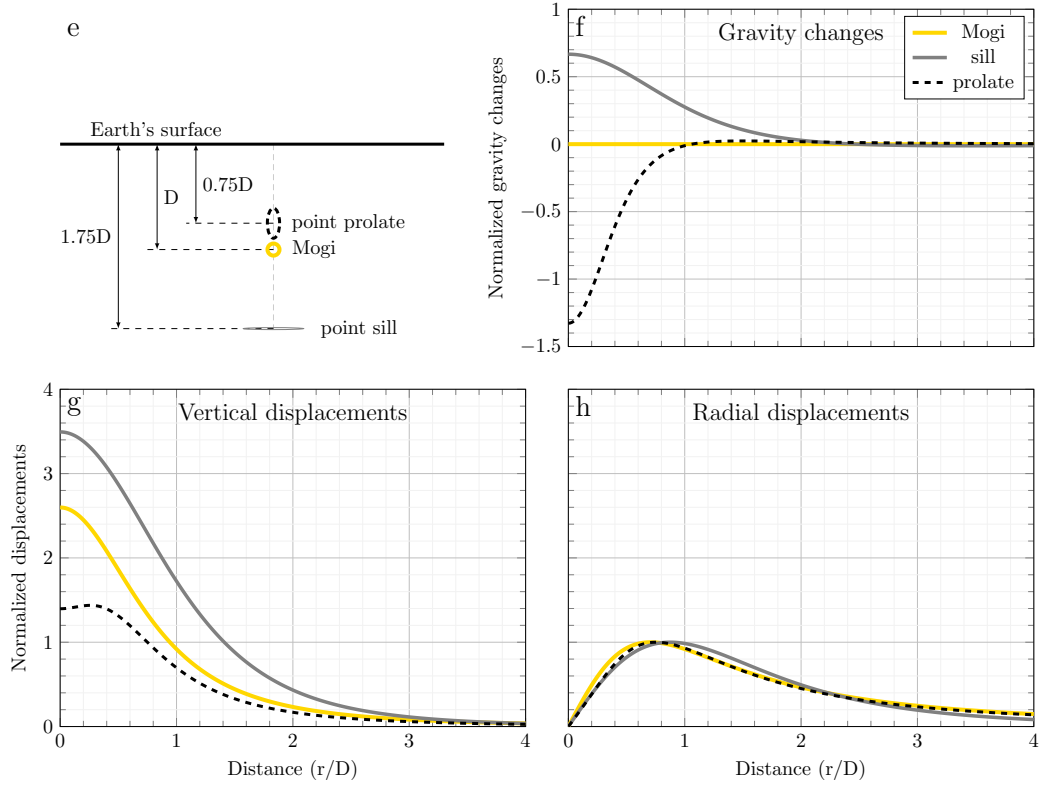

Similar radial displacements

Figure 4. Gravity changes ($\Delta g = \delta g - \Delta g_{\mathrm{FA}}$), vertical displacements (u_v) and radial displacements (u_r) for point sources of different aspect ratios and depths. For all sources $\Delta M = 0$. Top block: The sources illustrated in (a) give rise to different Δg (d), similar u_v (b), and different u_r (c). Bottom block: The sources in (e) cause different Δg (f), similar u_r (g), and different u_v (h). The potency vectors of the point spherical source, point prolate source and point sill in both (a) and (e) may be any positive multiple of $(1, 1, 1)$, $(1, 1, 0.44)$ and $(0, 0, 1)$, respectively. The gravity changes are normalized by the maximum Δg_{SM} (b and f) and the displacements are normalized by the maximum vertical displacement (c, d, g and h). All distances are normalized by the depth of the point spherical source, D.

The gravity change solutions for the point CDM, which we provide here, extend this potential to joint inversions of surface displacements and gravity changes. Volcanic deformation sources are often deep or far enough from the observation point to be treated as far field sources. The point CDM can provide a first order solution which can be later improved by more sophisticated numerical models. Some complexities such as layering or viscoelasticity can be accounted for (Amoruso et al., 2008) by using appropriate Green's functions for point dislocations (Okubo, 1993; Sun & Okubo, 1993; Wang et al., 2006). Besides, theory errors, arising from ignoring real Earth complexities, can be estimated in terms of noise covariance matrices within a Bayesian framework (see Minson et al., 2013; Duputel et al., 2014; Vasyura-Bathke et al., 2021).

Finite pressurized ellipsoidal cavities can be approximated by a set of point CDMs uniformly distributed in the cavity volumes. With a high number of point CDMs, this approach can be used for benchmarking numerical models. A few dozens of uniformly-distributed point CDMs provide satisfactory results for finite-source inversions (Amoruso et al., 2008). A practical compromise for finite pressurized ellipsoids at intermediate depths is the quadrupole approximation, which in its basic form involves seven point CDMs of appropriate potencies and locations on the axes of the ellipsoid (Amoruso & Crescentini, 2011).

We showed that by using our model it is possible to use either horizontal or vertical displacements along with the gravity changes to constrain all the deformation source parameters and the intrusion mass (Figure 4). The free-air and the surface mass contributions can be determined once the vertical displacements are known (equations 6 and 7). Measuring accurate vertical displacements along with gravity in real time monitoring is challenging. If the vertical displacements are not available or are inaccurate, the vertical displacements from the deformation model can be used within the inversion procedure to calculate the contributions above. We will explore this feature in a future study.

Fully coupled inversions of surface displacements and gravity changes constrain the deformation source parameters and the intrusion mass without making any assumption on the properties of the intruding fluid. The intrusion density can be estimated from the inferred mass only if the interface volume change, ΔV_{int}, is known (see equation 4) (ΔV_{int} should not be mistaken for the chamber volume change δV_{c}). It can be shown from equations (2) and (3) that the determination of ΔV_{int} requires knowledge of the fluid compressibility. This shows that unlike mass change estimates, the estimates of the intrusion density are prone to large uncertainties.

5 Conclusions

1. Surface gravity changes are sensitive to both the intruding fluid mass and the deformation-induced surface uplift (subsidence) and country rock dilatation. Due to this coupling between the gravity changes and host rock deformations, gravity changes can be used also to constrain deformation source parameters, namely, the location, spatial orientation and potency of triaxial source models for expanding reservoirs.

2. We provide analytical solutions and MATLAB codes for the surface displacements and gravity changes caused by the point CDM as a model for triaxial sources of expansion.

3. By using the point CDM, fully coupled inversions of surface displacements and gravity changes can now be performed. These inversions constrain the mass changes and deformation source parameters simultaneously.

4. The analytical solutions for the total gravity changes and individual gravity change contributions associated with the point CDM can be used to validate new semi-analytical and numerical gravity change models. By using a uniform distribution of multiple point CDMs, finite-source solutions with arbitrary accuracies can be achieved. A configuration of seven point CDMs according to the Amoruso and Cres-

centini (2011) quadrupole approximation provides an appropriate solution for inversions involving finite pressurized ellipsoidal sources at intermediate depths.

5. Joint inversions of gravity changes and either vertical or horizontal displacements can fully recover all the deformation source parameters and the intrusion mass. This implies that accurate horizontal displacements can cover for the lack of accurate vertical displacements at all stations of a monitoring network.

Appendix A Gravity changes caused by point tensile dislocations

Following the conventions in section 2 and based on Okubo (1991) expressions, a point tensile dislocation below the origin with depth d, azimuth 0, dip angle δ, potency ΔV and filled with an intrusion mass ΔM causes the gravity change contributions $\Delta g_{\Delta V}$, Δg_{MD}, Δg_{SM} and Δg_{FA} at $(x, y, 0)$, such that

$$
\begin{aligned}
\Delta g_{\Delta V} &= -G\rho_{\mathrm{r}}\Delta V \frac{d}{r^3}, \\
\Delta g_{\mathrm{MD}} &= G\rho_{\mathrm{r}}\Delta V(1-2\nu)\left[\frac{d}{r^3} - \frac{1}{r(r+d)} + \frac{x^2(2r+d)}{r^3(r+d)^2}\right]\sin^2\delta, \\
\Delta g_{\mathrm{SM}} &= 2\pi G\rho_{\mathrm{r}}\delta h, \\
\Delta g_{\mathrm{FA}} &= \gamma\delta h, \\
\Delta g_{\Delta M} &= G\Delta M\frac{d}{r^3},
\end{aligned}
\tag{A1}
$$

where $r = \left(x^2 + y^2 + d^2\right)^{1/2}$, and δh is the surface uplift associated with the point dislocation (see Okada, 1985; Okubo, 1991). It follows that

$$
\begin{aligned}
\Delta g &= \Delta g_{\Delta V} + \Delta g_{\mathrm{SM}} + \Delta g_{\mathrm{SM}}, \\
&= -G\rho_{\mathrm{r}}\Delta V\frac{d}{r^3}\left[1 - \frac{3}{r^2}(x\sin\delta + d\cos\delta)^2\right].
\end{aligned}
\tag{A2}
$$

References

Aki, K., & Richards, P. G. (2002). *Quantitative seismology* (2nd ed.). Sausalito, California: University Science Books.

Amoruso, A., & Crescentini, L. (2011). Modelling deformation due to a pressurized ellipsoidal cavity, with reference to the campi flegrei caldera, italy. *Geophysical Research Letters*, *38*(1).

Amoruso, A., & Crescentini, L. (2013). Analytical models of volcanic ellipsoidal expansion sources. *Annals of Geophysics*, *56*(4), 0435.

Amoruso, A., Crescentini, L., & Berrino, G. (2008). Simultaneous inversion of deformation and gravity changes in a horizontally layered half-space: evidences for magma intrusion during the 1982–1984 unrest at Campi Flegrei caldera (Italy). *Earth and Planetary Science Letters*, *272*(1-2), 181–188.

Battaglia, M., Gottsmann, J., Carbone, D., & Fernández, J. (2008). 4D volcano gravimetry. *Geophysics*, *73*(6), WA3–WA18.

Battaglia, M., Roberts, C., & Segall, P.   (1999).   Magma intrusion beneath Long Valley caldera confirmed by temporal changes in gravity.   *Science*, *285*(5436), 2119–2122.

Battaglia, M., Segall, P., & Roberts, C.   (2003).   The mechanics of unrest at Long Valley caldera, California. 2. Constraining the nature of the source using geodetic and micro-gravity data.   *Journal of Volcanology and Geothermal Research*, *127*(3-4), 219–245.

Battaglia, M., Troise, C., Obrizzo, F., Pingue, F., & De Natale, G.   (2006).   Evidence for fluid migration as the source of deformation at Campi Flegrei caldera (Italy). *Geophysical Research Letters*, *33*(1).

Beauducel, F., Peltier, A., Villié, A., & Suryanto, W.   (2020).   Mechanical imaging of a volcano plumbing system from GNSS unsupervised modeling.   *Geophysical Research Letters*, *47*(17), e2020GL089419.   doi: https://doi.org/10.1029/2020GL089419

Bonafede, M., & Ferrari, C.   (2009).   Analytical models of deformation and residual gravity changes due to a Mogi source in a viscoelastic medium. *Tectonophysics*, *471*(1-2), 4–13.

Bonafede, M., & Mazzanti, M.   (1998).   Modelling gravity variations consistent with ground deformation in the Campi Flegrei caldera (Italy).   *Journal of Volcanology and Geothermal Research*, *81*(1-2), 137–157.

Carbone, D., Antoni-Micollier, L., Hammond, G., Zeeuw-van Dalfsen, D., Rivalta, E., Bonadonna, C., . . . others   (2020).   The NEWTON-g gravity imager: towards new paradigms for terrain gravimetry.   *Frontiers in Earth Science*, *8*, 452.

Carbone, D., Cannavó, F., Greco, F., Reineman, R., & Warburton, R. J.   (2019).   The Benefits of Using a Network of Superconducting Gravimeters to Monitor and Study Active Volcanoes.   *Journal of Geophysical Research: Solid Earth*, *124*(4), 4035–4050. doi: 10.1029/2018JB017204

Carbone, D., Poland, M. P., Diament, M., & Greco, F.   (2017).   The added value of time-variable microgravimetry to the understanding of how volcanoes work.   *Earth-Science Reviews*, *169*, 146–179. doi: 10.1016/j.earscirev.2017.04.014

Charco, M., Camacho, A. G., Tiampo, K. F., & Fernández, J.   (2009).   Spatiotemporal gravity changes on volcanoes: Assessing the importance of topography.   *Geophysical research letters*, *36*(8).

Charco, M., Fernández, J., Luzón, F., & Rundle, J.   (2006).   On the relative importance of self-gravitation and elasticity in modeling volcanic ground deformation and gravity changes. *Journal of Geophysical Research: Solid Earth*, *111*(B3).

Charco, M., Tiampo, K. F., Luzón, F., & Fernández Torres, J.   (2005).   Modelling gravity changes and crustal deformation in active volcanic areas.   *Física de la Tierra*.

Creutzfeldt, B., Güntner, A., Wziontek, H., & Merz, B.   (2010).   Reducing local hydrology from high-precision gravity measurements: a lysimeter-based approach.   *Geophysical Journal International*, *183*(1), 178–187.

Currenti, G.   (2014).   Numerical evidence enabling reconciliation gravity and height changes in volcanic areas. *Geophysical Journal International*, *197*(1), 164–173. doi: 10.1093/gji/ggt507

Currenti, G.   (2018).   Viscoelastic modeling of deformation and gravity changes induced by pressurized magmatic sources.   *Journal of Volcanology and Geothermal Research*, *356*, 264–277.

Currenti, G., Del Negro, C., & Ganci, G.   (2007).   Modelling of ground deformation and gravity fields using finite element method: an application to Etna volcano.   *Geophysical Journal International*, *169*(2), 775–786.

Currenti, G., Del Negro, C., & Ganci, G.   (2008).   Finite element modeling of ground deformation and gravity field at Mt. Etna. *Annals of Geophysics*, *51*(1).

Davis, P. M.   (1986).   Surface deformation due to inflation of an arbitrarily oriented

triaxial ellipsoidal cavity in an elastic half-space, with reference to Kilauea volcano, Hawaii. *Journal of Geophysical Research: Solid Earth*, *91*(B7), 7429–7438.

Dieterich, J. H., & Decker, R. W. (1975). Finite element modeling of surface deformation associated with volcanism. *Journal of Geophysical Research (1896–1977)*, *80*(29), 4094–4102. doi: https://doi.org/10.1029/JB080i029p04094

Duputel, Z., Agram, P. S., Simons, M., Minson, S. E., & Beck, J. L. (2014, 01). Accounting for prediction uncertainty when inferring subsurface fault slip. *Geophysical Journal International*, *197*(1), 464–482. doi: 10.1093/gji/ggt517

Eshelby, J. D. (1957). The determination of the elastic field of an ellipsoidal inclusion, and related problems. *Proceedings of the royal society of London. Series A. Mathematical and physical sciences*, *241*(1226), 376–396.

Fernández, J., Tiampo, K. F., & Rundle, J. B. (2001). Viscoelastic displacement and gravity changes due to point magmatic intrusions in a gravitational layered solid earth. *Geophysical Journal International*, *146*(1), 155–170. doi: 10.1046/j.0956-540x.2001.01450.x

Fernández, J., Tiampo, K. F., Rundle, J. B., & Jentzsch, G. (2005). On the interpretation of vertical gravity gradients produced by magmatic intrusions. *Journal of Geodynamics*, *39*(5), 475–492.

Ferrari, C., Bonafede, M., & Trasatti, E. (2015). Relations between pressurized triaxial cavities and moment tensor distributions. *Annals of Geophysics*, *58*(4), 0438.

Güntner, A., Reich, M., Mikolaj, M., Creutzfeldt, B., Schroeder, S., Thoss, H., . . . Wziontek, H. (2017). Superconducting gravimeter data of iGrav006 and auxiliary hydro-meteorological data from Wettzell-Supplement to: Landscape-scale water balance monitoring with an iGrav superconducting gravimeter in a field enclosure.

Hagiwara, Y. (1977). The mogi model as a possible cause of the crustal uplift in the eastern part of izu peninsula and the related gravity change. *Bull. Earthq. Res. Inst.*, *52*, 301–309.

Ichihara, M., Kusakabe, T., Kame, N., & Kumagai, H. (2016). On volume-source representations based on the representation theorem. *Earth, Planets and Space*, *68*(1), 1–10. doi: 10.1186/s40623-016-0387-3

Kazama, T., Okubo, S., Sugano, T., Matsumoto, S., Sun, W., Tanaka, Y., & Koyama, E. (2015). Absolute gravity change associated with magma mass movement in the conduit of Asama Volcano (Central Japan), revealed by physical modeling of hydrological gravity disturbances. *Journal of Geophysical Research: Solid Earth*, *120*(2), 1263–1287.

Lien, T., Cheng, C.-C., Hwang, C., & Crossley, D. (2014). Assessing active faulting by hydrogeological modeling and superconducting gravimetry: A case study for Hsinchu Fault, Taiwan. *Journal of Geophysical Research: Solid Earth*, *119*(9), 7319-7335. doi: https://doi.org/10.1002/2014JB011285

Lisowski, M. (2007). Analytical volcano deformation source models. In *Volcano Deformation: Geodetic Monitoring Techniques* (pp. 279–304). Berlin, Heidelberg: Springer Berlin Heidelberg. doi: 10.1007/978-3-540-49302-0_8

Lisowski, M., Dzurisin, D., Denlinger, R. P., & Iwatsubo, E. Y. (2008). Analysis of GPS-measured deformation associated with the 2004–2006 dome-building eruption of Mount St. Helens, Washington. In *A Volcano Rekindled: The Renewed Eruption of Mount St. Helens, 2004–2006* (Vol. 1750, pp. 301–333). US Geological Survey Reston, Virginia.

Lundgren, P., Nikkhoo, M., Samsonov, S. V., Milillo, P., Gil-Cruz, F., & Lazo, J. (2017). Source model for the Copahue volcano magma plumbing system constrained by InSAR surface deformation observations. *Journal of Geophysical Research: Solid Earth*, *122*(7), 5729–5747.

Minson, S., Simons, M., & Beck, J. (2013). Bayesian inversion for finite fault earth-

quake source models I—Theory and algorithm. *Geophysical Journal International*, *194*(3), 1701–1726.

Mogi, K. (1958). Relations between the eruptions of various volcanoes and the deformations of the ground surfaces around them. *Earthq Res Inst*, *36*, 99–134.

Nikkhoo, M., Walter, T. R., Lundgren, P. R., & Prats-Iraola, P. (2017). Compound dislocation models (CDMs) for volcano deformation analyses. *Geophysical Journal International*, *208*(2), 877–894. doi: 10.1093/gji/ggw427

Okada, Y. (1985). Surface deformation due to shear and tensile faults in a half-space. *Bulletin of the seismological society of America*, *75*(4), 1135–1154.

Okubo, S. (1991). Potential and gravity changes raised by point dislocations. *Geophysical journal international*, *105*(3), 573–586.

Okubo, S. (1992). Gravity and potential changes due to shear and tensile faults in a half-space. *Journal of Geophysical Research: Solid Earth*, *97*(B5), 7137–7144.

Okubo, S. (1993). Reciprocity theorem to compute the static deformation due to a point dislocation buried in a spherically symmetric Earth. *Geophysical Journal International*, *115*(3), 921–928.

Okubo, S., Hirata, Y., Sawada, M., & Nagasawa, K. (1991). Gravity change caused by the 1989 earthquake swarm and submarine eruption off ito, japan test on the magma intrusion hypothesis. *Journal of Physics of the Earth*, *39*(1), 219–230.

Rivalta, E., & Segall, P. (2008). Magma compressibility and the missing source for some dike intrusions. *Geophysical Research Letters*, *35*(4).

Rundle, J. B. (1978). Gravity changes and the palmdale uplift. *Geophysical Research Letters*, *5*(1), 41–44.

Savage, J. (1984). Local gravity anomalies produced by dislocation sources. *Journal of Geophysical Research: Solid Earth*, *89*(B3), 1945–1952.

Segall, P. (2010). *Earthquake and volcano deformation.* Princeton University Press.

Sun, W., & Okubo, S. (1993). Surface potential and gravity changes due to internal dislocations in a spherical earth—I. Theory for a point dislocation. *Geophysical Journal International*, *114*(3), 569–592.

Trasatti, E., & Bonafede, M. (2008). Gravity changes due to overpressure sources in 3d heterogeneous media: application to campi flegrei caldera, italy. *Annals of Geophysics*.

Van Camp, M., Métivier, L., De Viron, O., Meurers, B., & Williams, S. (2010). Characterizing long-time scale hydrological effects on gravity for improved distinction of tectonic signals. *Journal of Geophysical Research: Solid Earth*, *115*(B7).

Vasyura-Bathke, H., Dettmer, J., Dutta, R., Mai, P. M., & Jonsson, S. (2021). Accounting for theory errors with empirical Bayesian noise models in nonlinear centroid moment tensor estimation. *Geophysical Journal International*, *225*(2), 1412–1431.

Walsh, J., & Rice, J. (1979). Local changes in gravity resulting from deformation. *Journal of Geophysical Research: Solid Earth*, *84*(B1), 165–170.

Wang, R., Lorenzo-Martin, F., & Roth, F. (2006). PSGRN/PSCMP—a new code for calculating co-and post-seismic deformation, geoid and gravity changes based on the viscoelastic-gravitational dislocation theory. *Computers & Geosciences*, *32*(4), 527–541.

Yang, X.-M., Davis, P. M., & Dieterich, J. H. (1988). Deformation from inflation of a dipping finite prolate spheroid in an elastic half-space as a model for volcanic stressing. *Journal of Geophysical Research: Solid Earth*, *93*(B5), 4249–4257. doi: 10.1029/JB093iB05p04249